Research Square

Preprints are preliminary reports that have not undergone peer review.
They should not be considered conclusive, used to inform clinical practice,
or referenced by the media as validated information.

High-Throughput Diffuse Electron Projection Lithography

Xianlong Wei

weixl@pku.edu.cn

Peking University https://orcid.org/0000-0002-1181-9500

Weilong Wu

Peking University

Yang Li

Peking University https://orcid.org/0009-0001-2387-1488

Shuyu Mao

Peking University

Fangyuan Zhan

Peking University

Yuqiang Yu

Peking University

Dan Su

Southeast University

Pan-Qin Sun

Southeast University

Bingjie Wang

Peking University

Taoyuan Zhu

Peking University

Ruixue Ding

Peking University

Ye Zhao

Peking University

Kechang Zhang

Peking University

Tong Zhang

Southeast University

Zhiwei Li

Peking University

Qing Chen

Peking University https://orcid.org/0000-0002-7919-5159

Article

Keywords:

Posted Date: April 22nd, 2026

DOI: https://doi.org/10.21203/rs.3.rs-9432451/v1

License: This work is licensed under a Creative Commons Attribution 4.0 International License.
Read Full License

Additional Declarations: There is **NO** Competing Interest.

High-Throughput Diffuse Electron Projection Lithography

Weilong Wu[1,#], Yang Li[1,#], Shuyu Mao[1], Fangyuan Zhan[1], Yuqiang Yu[1], Dan Su[2], Panqin Sun[2], Bingjie Wang[1], Taoyuan Zhu[1], Ruixue Ding[1], Ye Zhao[1], Kechang Zhang[1], Tong Zhang[2], Zhiwei Li[1,*], Qing Chen[1], Xianlong Wei[1,*]

[1]*Key Laboratory for the Physics and Chemistry of Nanodevices, School of Electronics, Peking University, Beijing 100871, China*

[2]*School of Electronic Science and Engineering, Southeast University, Nanjing 210096, China*

[#] These authors contributed equally

[*] Corresponding authors. Email: weixl@pku.edu.cn, lzw111@pku.edu.cn

ABSTRACT: Higher resolution and higher throughput are the relentless pursuits of lithography technologies for continued downscaling of semiconductor devices [1]. While the cutting-edge lithography technique for semiconductor manufacturing has evolved into extreme ultraviolet lithography (EUVL) [2, 3], there is still no foreseeable lithography techniques for post-EUVL [4]. Electron lithography, as a candidate for post-EUVL, exhibits higher resolution (down to sub-2 nm [5-7]) than that of EUVL, but encounters the main challenge of low throughput due to the trade-off between resolution and throughput resulting from the adoption of electron optics systems [8, 9]. Here, we report a diffuse electron projection lithography (DEPL) by adopting a wide diffuse electron beam in air as the exposure source and patterned monolayers of Au nanoparticles as the contact mask. Without the adoption of electron optics systems, the resolution and throughput of DEPL are decoupled and can be optimized independently. A minimum feature size of 4 nm and a throughput of 15 4-inch wafers per hour have been demonstrated by DEPL, with a potential throughput up to 532 12-inch wafers per hour. The outstanding features of high resolution, high throughput, and freedom from electron optics and ultrahigh vacuum systems make DEPL a promising and cost-effective lithography technique for post-EUVL.

Main Text

Fast developing in the emerging fields including artificial intelligence and automotive electronics drives the continued needs for faster, more power-efficient and cheaper chips, and thus continued needs for lithography techniques with higher resolution and higher throughput. The most advanced chips nowadays are manufactured based on extreme ultraviolet lithography (EUVL) [1, 2]. While the resolution of EUVL systems has reached 8 nm [10], close to the theoretical limit of ~5 nm considering a wavelength of 13.5 nm [11], it is urgent to develop lithography techniques with higher theoretical resolution and throughput than those of EUVL for satisfying continued needs for better chips in the era of post-EUVL. However, there is still no such a foreseeable candidate.

Electron beam lithography (EBL), as a potential lithography technique for post-EUVL, is well known for high resolution because of no constraint of diffraction limit [5-7]. However, EBL is inherently a slow exposure technology with low throughput, as it employs maskless serial writing exposure in contrast to parallel projection exposure in optical lithography. To increase throughput, electron beam of commercial EBL systems has evolved from single Gaussian beam, to single shaped beam, and to multi-beams today [12, 13]. As the cutting-edge EBL system, an EUVL mask writer system employs 590,000 electron beams with total beam current of 2.8 μA, but it still needs 12 hours to complete the exposure of an EUVL mask [14]. Therefore, the throughput of maskless EBL is currently more than 3 orders of magnitude lower than that required for high-volume semiconductor manufacturing. Several proof-of-concept systems of mask-based electron projection lithography (EPL) have been implemented since the 1970s to demonstrate the throughput required for semiconductor manufacturing [8, 15-16]. Similar to parallel exposure strategy in optical lithography, EPL employs a wide and uniform parallel electron beam to illuminate a stencil or scattering mask, and projects the image of mask onto the wafer. In the 1990s, EPL was studied as a potential lithography of semiconductor manufacturing for sub-100 nm feature size, and a feature size of 80 nm was experimentally demonstrated with 7.5 μA beam current [8].

Electron current landing on the exposed wafer is the most important figure of merit determining the throughput of electron lithography (EL) including both EBL and EPL systems. By adopting electron optics systems to form and project electron beams, the landing current and thus throughput of both EBL and EPL systems is fundamentally limited by stochastic Coulomb interactions between

electrons and lens aberrations of electron optics systems [8, 17-18]. High throughput and landing current imply high electron current density and thus strong stochastic Coulomb interactions, or large electron beam area and thus large lens aberrations. Strong stochastic Coulomb interactions and large lens aberrations further result in large image blur and poor resolution. A trade-off between resolution and throughput therefore exists for both EBL and EPL, which places a root constraint for them to achieve high resolution and high throughput at the same time. If an EL system were to achieve the same throughput as that of the cutting-edge EUVL system, namely 220 12-inch wafers per hour [19], the landing current is estimated to be 4.3 mA, assuming a resist sensitivity of 100 μC/cm^2 (refs. 20, 21) and neglecting overhead time. This is a huge current in comparison with the beam current of 2.8 μA for the cutting-edge EBL system [14] and 7.5 μA for the cutting-edge EPL system [8]. Therefore, to develop EL technologies for post-EUVL, the most important task is to search for a way of illuminating a wafer with the electron current of three orders of magnitude higher than those of the existing cutting-edge technologies, and at the same time without degrading the resolvable feature size.

Diffuse electron projection lithography (DEPL)

To address the challenge, here we report a diffuse electron projection lithography (DEPL), which adopts large-area uniform diffuse electron beam in air as the exposure source and patterned close-packed monolayers of Au nanoparticles as the contact mask (Fig. 1a). The diffuse electron source is generated by injecting high-energy electrons of 10-20 keV from vacuum into air through an array of membrane windows. Due to scattering by air molecules, electrons moving in air are slowed down, and show increasingly randomized distributions in position, direction and energy. At the position of several millimeters away from the membrane windows, where the wafer to be exposed is placed, a wide diffuse electron source with uniform spatial distribution in an area similar to that of the window array and an average energy of a few keV is formed.

Au nanoparticle monolayers with designed patterns and conformally contacting on the surface of resist are used as the mask in DEPL. Au nanoparticle monolayers block diffuse electrons from reaching the resist under them during exposure, and are rinsed away after exposure (Fig. 1b). The blocking capability of the mask depends on the thickness of Au nanoparticles and electron energy. An Au film with 20 nm thickness can block 46% electrons with energy of 5 keV (Supplementary Fig. S1). Employing the mask of 20 nm thick Au nanoparticle monolayers and a diffuse electron source with

average energy of 5 keV can therefore result in enough dose differences between exposed and masked areas if the resist with a contrast higher than 3.7 is used. The patterns of the mask are then transferred to the resist layer with 1:1 ratio after development (Fig. 1b). As Au nanoparticle monolayers show periodic variations in thickness, the dose of electrons reaching the resist under the mask show variations with the same period. Finer patterns with the period of nanoparticle diameter are therefore formed in designed patterns.

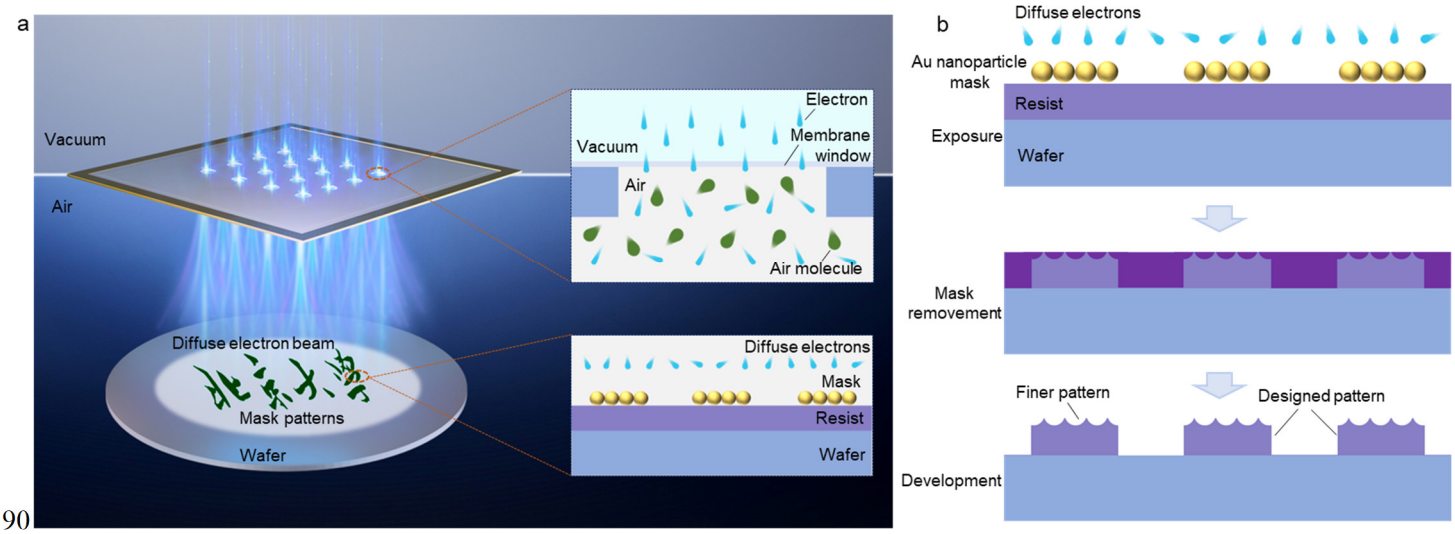


Fig. 1 | Schematic of diffuse electron projection lithography (DEPL). a, Schematic diagram illustrates DEPL by adopting a wide diffuse electron beam in air as the exposure source and patterned monolayers of Au nanoparticles as the contact mask. The diffuse electron source is generated by injecting high-energy electrons (10-20 keV) through an array of membrane windows from vacuum into air, where discrete electron beams are merged into a wide and uniform source by the scattering of air molecules. **b,** Schematic diagram illustrates the procedures of DEPL with positive resist. After exposure, mask removement and development, the patterns of the mask are transferred to the resist with 1:1 ratio.

In contrast to previous EL techniques [8, 15-16], where resolution and throughput are both primarily governed by electron optics systems with a trade-off between them, the resolution and throughput of DEPL are decoupled as no electron optics systems are used, and thus can be optimized independently. The resolution of EL with a contact mask is primarily determined by the minimum size of the mask. Adopting the contact mask of Au nanoparticle monolayers, DEPL exhibits a minimum feature size comparable to the diameter of Au nanoparticles in the case where the mask is one nanoparticle wide. The diameter of Au nanoparticles for self-assembled monolayers has reached sub-5 nm [22, 23]. Calculations show that an Au film with 5 nm thickness can block 44% electrons with energy of 2 keV (Supplementary Fig. S1). Therefore, the minimum feature size of 5 nm can be theoretically realized

by employing the monolayers of 5-nm-thick Au nanoparticles as the mask and a diffuse electron source with average energy of 2 keV.

The throughput of DEPL can be optimized by increasing the landing current of diffuse electron source. The area of a diffuse electron source is primarily determined by that of the membrane window array, which is fabricated on a Si chip and can show an area up to that of a whole Si wafer, and can be more than three orders of magnitude larger than those (~1 mm^2) of previous EPL systems [8, 16]. The enormous boost in illumination area of electron sources makes it feasible for DEPL to exhibit the large landing current and throughput required for semiconductor manufacturing. With decoupled resolution and throughput, our DEPL provides a way of realizing both small feature size and high throughput as required for semiconductor manufacturing.

Diffuse electron sources

To generate a diffuse electron source in experiments, free electrons are firstly emitted from a thermionic electron emitter and accelerated to more than 10 keV in a vacuum chamber by an accelerating voltage V_{acc}. Then they are injected into ambient air through a 4×4 array of 1.4-mm-spaced Si_3N_4 membrane windows (Fig. 2a-b), which are fabricated on a 20×20 mm^2 Si chip. The Si_3N_4 membrane windows should be transparent enough for high-energy electrons, and at the same time robust enough to withstand atmospheric pressure. To meet the requirements, Si_3N_4 membrane windows are designed to show an area of 1.1×1.1 mm^2 and a thickness of 200 nm (Fig. 2b).

The spatial distributions of a diffuse electron source are recorded by a fluorescent screen, and are observed to strongly depend on the distance (d) from the window chip (Fig. 2c). At d=1 mm, electrons mainly distribute near the membrane windows where they exited, with a distribution profile clearly showing the array of discrete beams and non-uniform density for different beams. When d increases to 3 mm, the discrete beams emitted from different membrane windows merge into a wide and continuous beam with more uniform distribution due to scattering by air molecules. Notably, at d=5 mm, the source with V_{acc}=18 kV evolves into a wide circular beam with highly uniform distribution in an area similar to that of the whole window arrays, namely ~9 mm in diameter. The randomization induced by air molecule scattering therefore can merge an array of discrete and non-uniform beams into a wide uniform beam. It provides an effective method for generating large-area uniform electron source as required by EPL.

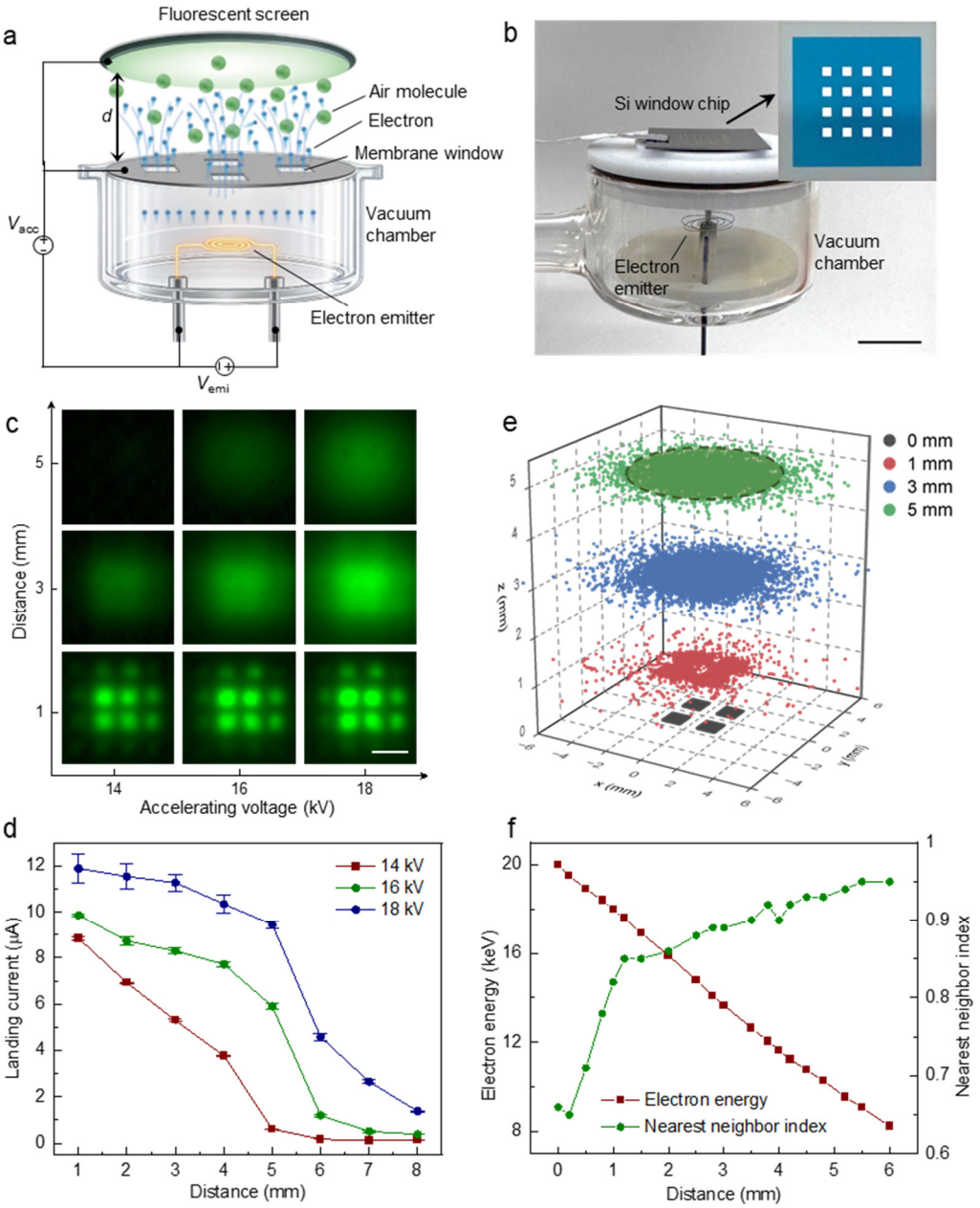


Fig. 2 | Diffuse electron sources for DEPL. a, Schematic of the apparatus for generating and visualizing a diffuse electron source. It mainly consists of a glass vacuum chamber, a thermionic electron emitter, a Si chip with an array of Si_3N_4 membrane windows and a fluorescent screen. Electrons are emitted from the emitter by applying V_{emi} to it and accelerated in vacuum by applying V_{acc} between the electron emitter and window chip. The distance between the fluorescent screen or exposed wafer and membrane windows is d. **b,** Photograph of the apparatus with the fluorescent screen not shown. The inset shows the Si chip consisting of an array of 4×4 Si_3N_4 membrane windows in an area of 8.6×8.6 mm^2. **c,** Fluorescence images on the fluorescent screen showing the spatial distributions of diffuse electron sources with d=1, 3 and 5 mm, and V_{acc}=14, 16 and 18 kV. **d,** Landing current of the diffuse electron source measured at different d with V_{acc}=14, 16 and 18 kV for fixed emission current of 80 μA from the emitter. Each data point shows the averaged value from 5 repeated measurements with error bar being standard deviation. **e**, Simulated spatial distributions of a diffuse electron source with d=1, 3 and 5 mm. **f,** Simulated average electron energy and nearest neighbor index

of a diffuse electron source varying with *d*. The simulations in **e** and **f** are based on Monte Carlo simulations and V_{acc}=20 kV. Scale bars: 10 mm (**b**), 4 mm (**c**).

As judged from the decreased brightness in fluorescent screen, the density of electrons in diffuse sources decreases with *d* increase, and electrons with higher initial energies can penetrate farther in air. This is in good agreement with the measurement of landing current (Fig. 2d), which is observed to decrease with *d* increase. While the landing current decreases to nearly zero at *d*= 6 mm for V_{acc}=14 kV, electrons with V_{acc}=18 kV can penetrate more than 8 mm in air. For an emission current of 80 μA from the emitter, the landing current is measured to be 9.4 μA at *d*=5 mm and with V_{acc}=18 kV, which corresponds to a current density of 14.8 μA/cm^2 considering a beam diameter of 9 mm. The landing current is also observed to increase with the increase of V_{acc} for fixed emission current due to enhanced transmission of electrons through the window chip.

The merging of discrete beams into a wide and uniform diffuse source by the scattering of air molecules is reproduced by modeling the transport in air of 20 keV electrons, which are injected into air from a 2×2 array of 1-mm-wide and 1-mm-spaced windows (Fig. 2e). In good agreement with the experimental observations, the simulated electron distributions show clear profile of discrete beams at *d*=1 mm, and merge into one circular uniform beam with an area similar to that of the whole beam array at *d*=3 mm. When *d* increases to 5 mm, the area of uniform beam further increases with a decreased density. The average electron energy of the diffuse source is simulated to decrease approximately linearly with *d* at a rate of nearly 2 keV/mm (Fig. 2f). The average energy of diffuse electron sources can therefore be conveniently adjusted by changing the distance from the window chip.

Nearest neighbor index (NNI) is adopted to quantitatively analyze the randomness of the simulated spatial distributions of a diffuse electron source (Fig. 2f) [24]. NNI of the diffuse electron source is found to increase with *d* increase and approach 1, indicating that the spatial distribution of diffuse electron sources becomes more and more random as electrons move farther in air. While a NNI value of 1 implies complete spatial randomness with the same electron density across the beam (Supplementary Fig. S2), a NNI value of 0.95 at *d* = 5.5 mm indicates nearly complete spatial randomness for the distribution of the simulated diffuse electron source. The NNI analysis further confirms the feasibility of generating a wide uniform diffuse electron source by merging discrete beams through the random scattering of air molecules.

Contact mask of Au nanoparticle monolayers and chip-scale pattern transfer by DEPL

The contact mask of Au nanoparticle monolayers is prepared via a transfer printing method (Fig. 3a and Supplementary Fig. S3) [25, 26]. With the method, the mask of Au nanoparticle monolayers exhibits the same patterns as those on the PDMS stamp with 1:1 ratio. To demonstrate chip-scale pattern transfer by DEPL, a 10×10 mm^2 Si chip coated with about 200 nm thick PMMA film as the resist was used for DEPL. Fig. 3b shows as-prepared mask on the resist with the patterns of periodic circles with a diameter of 240 nm and a period of 500 nm. Each circle in the mask consists of close-packed Au nanoparticles with a diameter of about 20 nm (Fig. 3c). Exposure of the masked chip was performed by placing it against the diffuse electron source in Fig. 2.

The same patterns as those of the mask with periodic circles are obtained in the resist after development (Fig. 3e), demonstrating high fidelity of pattern transfer by DEPL. It is noteworthy that, the mask of Au nanoparticle monolayers shows triangular voids with the side length about 10 nm at the center of each nanoparticle triplet (Fig. 3d). The high fidelity of the designed circular patterns is attributed to the random moving directions of electrons in diffuse electron sources. As only electrons moving approximately perpendicular to the chip can penetrate the voids without blocking, most electrons in the diffuse electron source encounter blocking at the voids. The adoption of diffuse electron sources is therefore crucial for achieving the high-fidelity transfer of designed patterns when using the voided nanoparticle monolayers as the mask.

In addition to designed patterns of periodic circles, finer periodic patterns resulting from the periodic variations in the thickness of nanoparticle monolayers are observed in each designed circular patterns as expected (Fig. 3f). The finer periodic patterns show a period of about 20 nm, same as the diameter of nanoparticles. A minimum feature size of 4 nm, which is close to the reported resolution limit of EBL [6], is obtained in the finer periodic pattern (Fig. 3g). Even though the minimum feature size is not obtained from designed patterns, it places an achievable feature size of DEPL for designed patterns if designed masks with small enough sizes can be prepared.

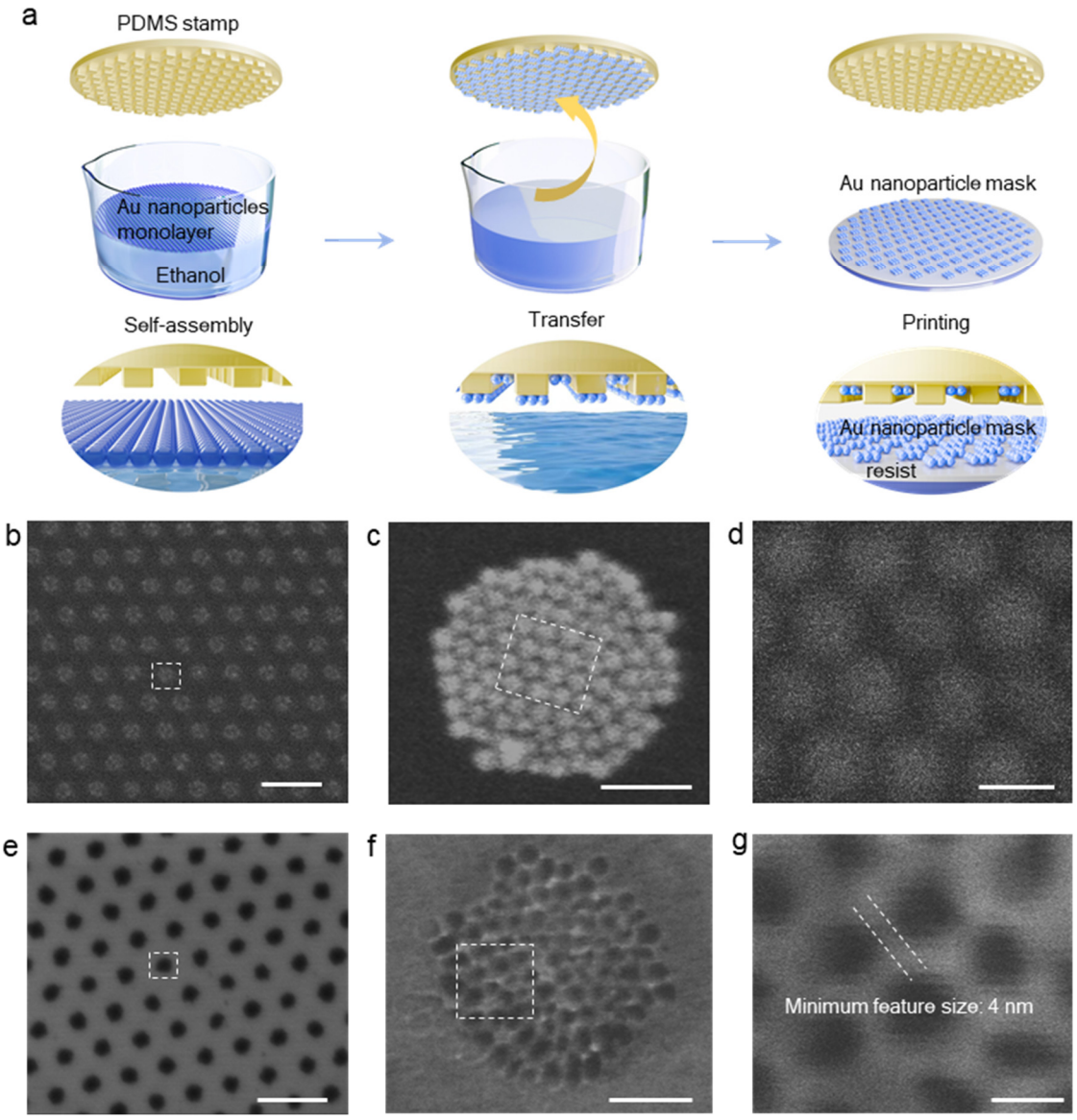


Fig. 3 | Contact mask of Au nanoparticle monolayers and chip-scale DEPL. a, Schematic diagram showing the processes of preparing the contact mask of Au nanoparticle monolayers. A close-packed monolayer of Au nanoparticles is firstly self-assembled at the ethanol/n-hexane biphasic interface, and then is transferred onto a PDMS stamp with designed patterns by contacting the stamp on the Au nanoparticle monolayer, and finally is transferred onto the surface of the resist by printing the stamp on the resist. **b,** Scanning electron microscopy (SEM) image showing as-prepared contact masks on the PMMA resist. **c,** SEM image of the framed area in **b** showing a close-packed monolayer of 20-nm-thick Au nanoparticles. **d,** SEM image of the framed area in **c** showing the presence of voids in the close-packed nanoparticle monolayer. **e**, SEM image of the patterns in the resist after pattern transfer by DEPL, showing the same periodic patterns as in **b**. **f**, SEM image of the framed area in **e** showing similar periodic patterns with **c**. **g**, SEM image of the framed area in **f** showing a minimum feature size of 4 nm**.** The exposure of the patterns in **e-j** was performed with V_{acc}=20 kV and d= 6 mm. Scale bars: 1 μm (**b**, **e**), 100 nm (**c**, **f**), 20 nm (**d**, **g**).

Wafer-scale pattern transfer by DEPL

To demonstrate wafer-scale lithography capability of DEPL, multiscale resist patterns were obtained on a 4-inch Si wafer by scanning a narrow diffuse electron source across the wafer with multiscale masks (Fig. 4a-d). The masks of the multiscale patterns show macroscopic form of Chinese characters for Peking University (Fig. 4e, Supplementary Fig. S4), and are composed of microscale periodic circles with a diameter of 3 μm and a period of 8 μm (Fig. 4f). Both macroscopic patterns of Chinese characters (Fig. 4g) and microscale patterns of periodic circles (Fig. 4h) are reproduced after development, indicating successful wafer-scale pattern transfer by DEPL. The height profile of microscale circular patterns in resist shows exact diameter and period as those of the mask patterns (Fig. 4h), indicating good fidelity of wafer-scale pattern transfer by DEPL. The iridescence of the multiscale patterns after development in Fig. 4g is attributed to the structural coloration arising from the diffraction of light by the periodic microscale patterns. The entire wafer was exposed with a total exposure time of 4 minutes, achieving a throughput of 15 wafers per hour.

The throughput of DEPL is primarily determined by the landing current, which can be limited by the electron emitter and membrane windows in the diffusion electron source. Without stringent requirements on the brightness, monochromaticity and size of electron emitters as in traditional EL with electron optics systems [27, 28], the electron emitter of a diffuse electron source can easily provide enough current required for high-throughput DEPL. Taking the emitter in Fig. 4b as an example, it can emit an electron current of more than 600 mA (Supplementary Fig. S5). The throughput of DEPL is thus mainly limited by the membrane windows, the most delicate components in the diffuse electron source. The impact of high-energy electrons on the windows may cause window failure because of temperature and stress increase, which places a limit on the maximum current density that the window chip can withstand. Fortunately, the membrane window chip work in air in DEPL, which can significantly facilitate thermal dissipation and minimize the limitation.

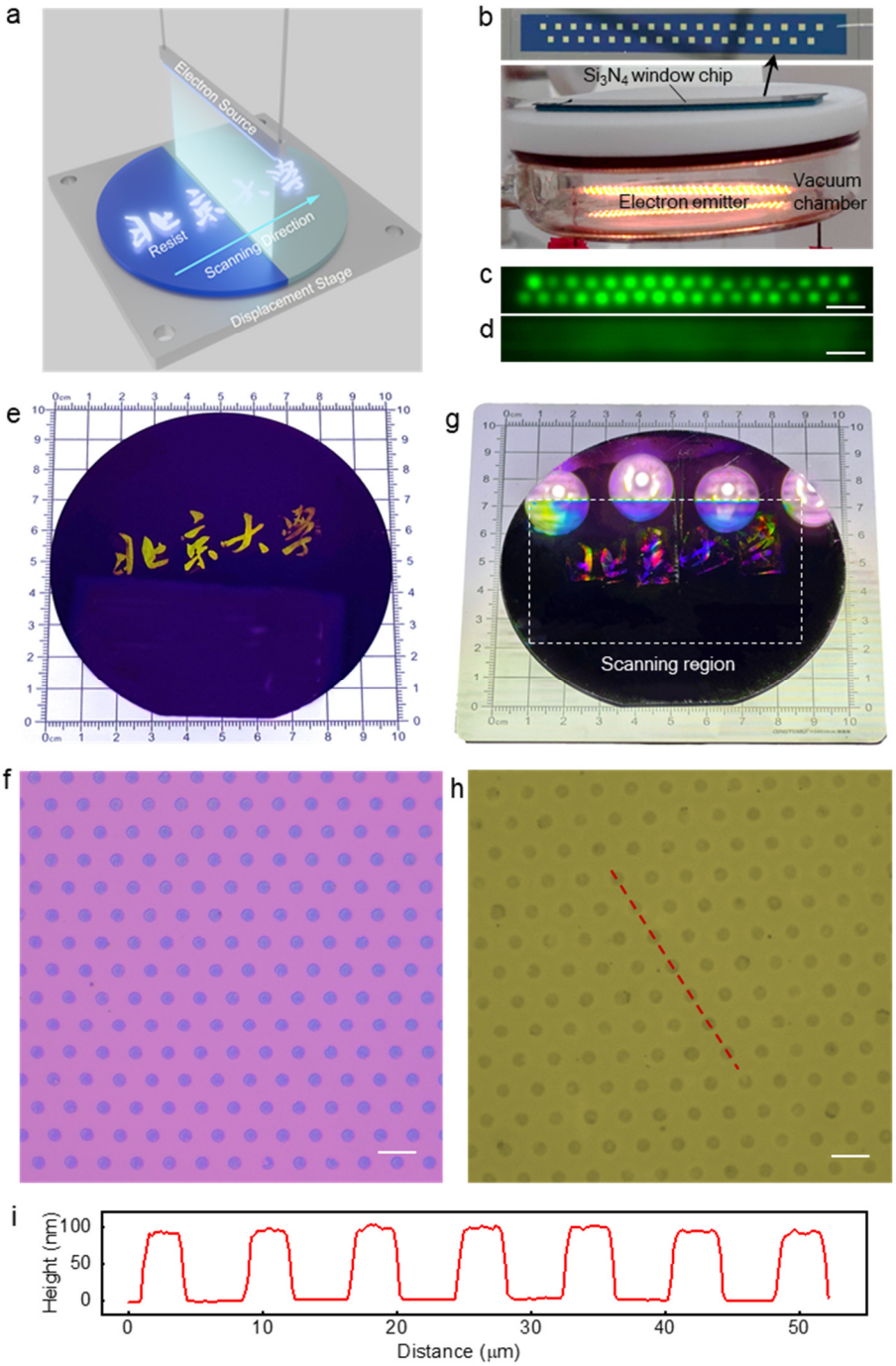


Fig. 4 | Wafer-scale DEPL of multiscale patterns. a, Schematic illustration showing wafer-scale DEPL by scanning a narrow diffuse electron source across the wafer. **b,** Photograph of the apparatus for generating the narrow diffuse electron source. It consists of a 50-mm-long thermionic electron emitter and a Si chip with two rows of Si_3N_4 windows in an area of 3.5×52 mm^2. **c-d,** Fluorescence images showing the spatial distributions of the diffuse electron source with d=1 mm (**c**), 3 mm (**d**) and V_{acc}=16 kV. **e-f,** Multiscale mask of Au nanoparticle monolayers on a 4-inch silicon wafer with resist layer. The multiscale mask shows macroscopic patterns (**e**) of Chinese characters for Peking University, and microscopic patterns (**f**) of periodic circles. **g-h,** Multiscale resist patterns obtained by DEPL based on the multiscale mask in **e-f**. Both macroscopic patterns (**g**) of Chinese characters for Peking University, and microscopic patterns (**h**) of periodic circles are reproduced in good fidelity. The four

bright circles in **g** are the reflections of the light sources for photography. **i,** Atomic force microscopy height profile of the microscale resist patterns along the dashed line in **h**. The wafer-scale exposure was performed with V_{acc}=16 kV and d= 3 mm. Scale bars: 6 mm (**c**, **d**), 10 μm (**f**, **h**).

For a specific current density, the landing current of a diffuse electron source is limited by the area of membrane window arrays, which can be scaled up to the area of a whole wafer (Supplementary Fig. S6). Applying the landing current density of 14.8 μA/cm² as measured for the diffuse electron source in Fig. 2d, the landing current of a diffuse electron source can reach up to 10.4 mA if an array of membrane windows in 12-inch is used. Assuming a resist sensitivity of 100 μC/cm^2 (refs. 20, 21) and neglecting overhead time, the landing current of 10.4 mA can result in a throughput up to 532 12-inch wafers per hour, more than two times larger than that of the cutting-edge EUVL [19]. The throughput can be further increased by increasing the landing current density that was not optimized in our experiments.

Discussion

In addition to realizing small feature size and high throughput simultaneously, DEPL shows several more beneficial features compared with previous EL techniques. First, DEPL is essentially a low energy lithography with electron energies of a few keV. Low electron energy can increase the resist sensitivity and throughput [29, 30], decrease the proximity effects [31], and reduce irradiation damage to the underlying substrate [32]. Second, the exposure is performed in ambient air. The feature can mitigate the heating and charging effects of the resist and mask [33, 34], which are significant for high-throughput electron lithography performed in vacuum and can seriously degrade resolution [35, 36]. It also eliminates the requirement on vacuum compatibility of the resist and exposed samples, enabling DEPL to pattern with volatile resists and wet samples [37]. Third, unlike traditional EBL which requires precisely focusing an electron beam onto the sample surface, DEPL is a focus-free technique using randomly moving electrons. The feature can eliminate the requirement on the flatness of the samples, making it convenient to perform DEPL on nonplanar and irregular surfaces [38].

Fourth, a conformal contact mask of Au nanoparticle monolayers is used. Compared with non-contact stencil or scattering masks in previous EPL [15, 16], it shows advantages of smaller feature size, higher fidelity and lower cost. Importantly, the mask deformation under dense and energetic electron irradiation, which is one of the main challenges for previous EPL [8, 39], can be minimized for our contact

mask working in air. Fifth, DEPL enables the exposure of a whole wafer in a single shot if a diffuse electron source with the size of a whole wafer is used. The feature can eliminate the overhead time for exposure field switching, the need for field stitching, and minimize the requirements on the moving of wafer stage. Lastly, no complex electron optics system and ultra-high vacuum system are used. Electron emitter is the only component that needs to work in vacuum in our DEPL system. Without stringent requirements on the brightness, monochromaticity and size, normal thermionic electron emitters with vacuum requirement of 10^{-3} Pa can be used. Free of complex electron optics system and ultra-high vacuum system makes our DEPL system much more compact and cost-effective than previous EBL and EPL systems.

In conclusion, a new electron lithography technique, named as diffuse electron projection lithography (DEPL), is developed by adopting diffuse electrons in air as the exposure source and patterned nanoparticle monolayers as the contact mask. Free of electron optics systems, DEPL exhibits no trade-off between resolution and throughput, enabling independent optimizations of the two important figures of merit. It provides an effective way of illuminating a wafer with the electron current of three orders of magnitude higher than those of the existing cutting-edge technologies and at the same time without degrading the resolution. It is demonstrated to exhibit a small feature size of 4 nm and a potential throughput of 532 12-inch wafers per hour, showing both higher resolution and higher throughput than those of EUVL. The outstanding features of both high resolution and high throughput, freedom from electron optics system and ultrahigh vacuum system make DEPL not only a technically viable solution for post-EUVL lithography, but also an economically attractive alternative that could democratize advanced nanofabrication beyond the realm of leading-edge semiconductor fabs.

Methods

Diffuse electron sources for DEPL

The vacuum chamber for electron emission and acceleration was maintained at a pressure about 10^{-3} Pa by a vacuum system. Thermionic emitters made of Ir-Y_2O_3 were used for electron emission. Spatial distributions of diffuse electron sources were recorded by a ZnO:Zn fluorescent screen. To eliminate fluorescent signals resulted from the incandescent thermionic emitter, they were first recorded by turning on the emitter but without applying the accelerating voltage V_{acc}, and then subtracted from those with the accelerating voltage applied. Landing current was measured by placing a metal electrode larger than the area of diffuse electron source against the source. To eliminate current of secondary electrons and ions, the electrode was grounded same as the Si chip with Si_3N_4 membrane windows. Membrane window chips were fabricated from a 4-inch Si wafer with 200 nm Si_3N_4 film on both sides (see Supplementary Fig. S6).

Contact mask of Au nanoparticle monolayers for DEPL

To prepare self-assembled monolayers of Au nanoparticles, eight milliliters of cetyltrimethylammonium bromide (CTAB)-capped Au nanoparticle solution (20 nm diameter, homogeneity CV%: 5%; 0.075 mg/ml Au, 50 mM CTAB) was firstly placed in a 50-ml glass bottle. Subsequently, 25 ml of 1H, 1H, 2H, 2H-perfluorodecanethiol (PFT) solution (10 mM, $V_{ethanol}$:V_{hexane} = 2:1) was poured into the Au nanoparticle solution. Vigorous agitation for 3 s resulted in the formation of a densely packed Au nanoparticle monolayer at the interface. Patterned PDMS stamps were fabricated via soft lithography using a silicon master. The assembled Au nanoparticle monolayers were transferred onto the PDMS stamp using the Langmuir–Schaefer technique. The contact mask of Au nanoparticle monolayers was then obtained by pressing the PDMS stamp against the resist film on silicon substrate with a uniform pressure of about 1×10^4 N/m^2 for 1 min to ensure conformal contact. The contact mask of multiscale patterns was prepared by an Intaglio-assisted transfer printing method (see Supplementary Fig. S4).

DEPL setup and processes

DEPL was performed with a home-made setup (see Supplementary Fig. S7), which mainly consists of a diffuse electron source, a vacuum system for maintaining vacuum required by the electron emitter, a three-axis translation stage driven by a brushless motor (Oriental Motor BMUD30-C2) for fixing and scanning the wafer, and a high voltage source for driving electron emission and accelerating electrons (Wisman XPG50N100). PMMA (950k A4, Sawatec SM-200) was used as the resist, and was spin-coated onto the substrate at 4000 r.p.m. followed by a bake at 170 °C for 3 min on a hot plate (Sawatec

HP-200). After exposure, the mask of Au nanoparticle monolayers was removed by immersing the substrate in a potassium monoiodide solution for 30 s. Exposed patterns were developed in developer (IPA:MIBK=3:1) for 90 s and immediately transferred to isopropanol (IPA) for 2 min to arrest development.

Monte Carlo simulations

Electron transport in ambient air and the blocking of electrons by Au nanofilms were simulated using the GAMOS 6.2.0 framework based on the Geant4 kernel. To simulate electron transport in ambient air, electrons with kinetic energy of 20 keV are uniformly injected into air through a 2×2 array of 1-mm-wide and 1-mm-spaced membrane windows. To characterize beam evolution, virtual scoring planes were positioned at varying propagation distances to record electron position, energy, and direction. A total number of 10,000 transport trajectories were computed and visualized using Castle Model Viewer. To simulate the blocking of electrons by Au nanofilms, electrons with energies of 2, 5, and 10 keV were simulated to transmit through uniform Au nanofilms with varying thicknesses and an area of 10×10 cm^2. A collection plane was defined behind the Au nanofilm closely to record the transmitted electrons. The beam-blocking efficacy was then derived by statistically analyzing the kinematic profiles of the electrons arriving at the collection plane.

References

1. Schoot, J. V. Exposure tool development toward advanced EUV lithography: a journey of 40 years driving Moore's law. *IEEE Electron Devices Magazine* **2**, 8–22 (2024).
2. Kaiser, W. The evolvement of lithography optics towards advanced EUV lithography: enabling the continuation of Moore's law for six decades. *IEEE Electron Devices Magazine* **2**, 23–34 (2024).
3. Van De Kerkhof, M. et al. Enabling sub-10nm node lithography: presenting the NXE:3400B EUV scanner. *Proc. SPIE* **10143**, 101430D (2017).
4. Kazazis, D., Santaclara, J. G., Van Schoot, J., Mochi, I. & Ekinci, Y. Extreme ultraviolet lithography. *Nat. Rev. Methods Primers* **4**, 84 (2024).
5. Manfrinato, V. R. et al. Aberration-corrected electron beam lithography at the one nanometer length scale. *Nano Lett.* **17**, 4562–4567 (2017).
6. Saifullah, M. S. M. et al. Patterning at the resolution limit of commercial electron beam lithography. *Nano Lett.* **22**, 7432–7440 (2022).
7. Saifullah, M. S. M. et al. Approaching angstrom-scale resolution in lithography using low-molecular-mass resists (<500 Da). *ACS Nano* **18**, 24076–24094 (2024).
8. R. S. Dhaliwal. Prevail—electron projection technology approach for next-generation lithography. *IBM J. Res. Dev.* **45**, 615–638 (2001).
9. Garcia, R., Knoll, A. W. & Riedo, E. Advanced scanning probe lithography. *Nat. Nanotechnol.* **9**,

577–587 (2014).
10. Gysen, A. C., van Loo, H., van Setten, E. & Yegen, G. High-resolution lithography: latest generation in EUV lithograph with 0.55 NA. *Proc. SPIE* **PC13215**. PC1321505 (2024).
11. Levinson, H. J. Challenges and limits to patterning using extreme ultraviolet lithography. *J. Micro/Nanopatterning, Mater., Metrol.* **24**, 011005 (2024).
12. Tomandl, M. et al. Multi-beam mask writing opens up new fields of application, including curvilinear mask pattern for high numerical aperture extreme ultraviolet lithography. *J. Micro/Nanopatterning, Mater., Metrol.* **23**, 011205 (2024).
13. Pfeiffer, H. C. Direct write electron beam lithography: a historical overview. *Proc. SPIE* **7823**, 782316 (2010).
14. Elmar Platzgumme. Multi-beam mask writers in the high-NA EUV era. *Proc. SPIE* **13216**, 1321616 (2024).
15. Heritage, M. B. Electron-projection microfabrication system. *J. Vac. Sci. Technol.* **12**, 1135–1140 (1975).
16. Harriott, L. R. Scattering with angular limitation projection electron beam lithography for suboptical lithography. *J. Vac. Sci. Technol. B* **15**, 2130–2135 (1997).
17. Stickel, W. Simulation of Coulomb interactions in electron beam lithography systems—a comparison of theoretical models. *J. Vac. Sci. Technol. B* **16**, 3211–3214 (1998).
18. Jansen, G. H. Trajectory displacement effect in particle projection lithography systems: modifications to the extended two-particle theory and Monte Carlo simulation technique. *J. Appl. Phys.* **84**, 4549–4567 (1998).
19. Klomp, P. 0.33 NA EUV systems for high-volume manufacturing. *Proc. SPIE* **PC13424**, PC134240G (2025).
20. Yamamoto, K. et al. Study of EB resist dissolution contrast and chemical blur impact on the ultimate resolution. *Proc. SPIE* **12293**, 122930N (2022).
21. Saito, M., Ugajin, K., Yagawa, K., Suenaga, M. & Kobayashi, Y. The performances and challenges of today's EB lithography and EB-resist materials. *J. Photopolym. Sci. Technol.* **27**, 511–516 (2014).
22. Yao, C., Yan, W., Dong, R., Dou, S. & Yang, L. Superlattice assembly strategy of small noble metal nanoparticles for surface-enhanced Raman scattering. *Commun. Mater.* **5**, 65 (2024).
23. Zeng, C., Chen, Y., Kirschbaum, K., Lambright, K. J. & Jin, R. Emergence of hierarchical structural complexities in nanoparticles and their assembly. *Science* **354**, 1580–1584 (2016).
24. Clark, P. J. & Evans, F. C. Distance to nearest neighbor as a measure of spatial relationships in populations. *Ecology* **35**, 445–453 (1954).
25. Schmid, H. et al. Preparation of metallic films on elastomeric stamps and their application for contact processing and contact printing. *Adv. Funct. Mater.* **13**, 145–153 (2003).
26. Song, L. et al. Instant interfacial self-assembly for homogeneous nanoparticle monolayer enabled conformal "lift-on" thin film technology. *Sci. Adv.* **7**, eabk2852 (2021).
27. Gaertner, G., Knapp, W. & Forbes, R. G. *Modern Developments in Vacuum Electron Sources*

Preface (Springer, Cham, 2020).
28. Golladay, S. D., Kendall, R. A. & Doran, S. K. High emittance source for the PREVAIL projection lithography system. *J. Vac. Sci. Technol. B* **17**, 2856–2859 (1999).
29. Manfrinato, V. R. et al. Sub-5keV electron-beam lithography in hydrogen silsesquioxane resist. *Microelectron. Eng.* **88**, 3070–3074 (2011).
30. Sun, X., Yao, G., Zheng, R., Zhao, D. & Qiu, M. Multiexposure grayscale patterns with low-energy electrons. *ACS Appl. Mater. Interfaces* **17**, 5232–5238 (2025).
31. Peterson, P. A., Radzimski, Z. J., Schwalm, S. A. & Russell, P. E. Low-voltage electron beam lithography. *J. Vac. Sci. Technol. B* **10**, 3088–3093 (1992).
32. Krasheninnikov, A. V. & Banhart, F. Engineering of nanostructured carbon materials with electron or ion beams. *Nat. Mater.* **6**, 723–733 (2007).
33. Lu, Y. & Lal, A. Vacuum-free self-powered parallel electron lithography with sub-35-nm resolution. *Nano Lett.* **10**, 2197–2201 (2010).
34. Donald, A. M. The use of environmental scanning electron microscopy for imaging wet and insulating materials. *Nat. Mater.* **2**, 511–516 (2003).
35. Ikari, Y., Okamoto, K., Konda, A., Kozawa, T. & Tamura, T. Heating effect of the radiation chemistry of polyhydroxystyrene-type chemically amplified resists. *Jpn. J. Appl. Phys.* **59**, 086506 (2020).
36. Zhang, J., Fouad, M., Yavuz, M. & Cui, B. Charging effect reduction in electron beam lithography with nA beam current. *Microelectron. Eng.* **88**, 2196–2199 (2011).
37. Dhand, A. P., Davidson, M. D. & Burdick, J. A. Lithography-based 3D printing of hydrogels. *Nat. Rev. Bioeng.* **3**, 108–125 (2024).
38. Zhu, C., Ekinci, H., Pan, A., Cui, B. & Zhu, X. Electron beam lithography on nonplanar and irregular surfaces. *Microsyst. Nanoeng.* **10**, 52 (2024).
39. Martin, C. J., Engelstad, R. L., Lovell, E. G. & Liddle, J. A. Thermomechanical modeling of the SCALPEL mask during exposure. *Proc. SPIE* **3997**, (2000).

Acknowledgments

We thank L.S., Y.H. (Hangzhou Normal University) for assistance with Au nanoparticle self-assembly, Y.L. (Peking University) for the assistance of the MC simulations. We acknowledge the technical support provided by the Nanofabrication Laboratory at Peking University and the Microfabrication Platform for Nano-Optoelectronics. This work was supported by the National Natural Science Foundation of China (Grant No. 62350040 to X.W. and 62401019 to Z.L.).

Author contributions

X.W. conceived the idea and supervised the investigation. W.W., X.W., Z.L., Y.L. and Y.Y. designed and constructed the experimental setup. W.W., Y.L. and F.Z. conducted PEBL experiments. Y.L., Z.L.,

S.M. and W.W. designed and prepared Si window chips and diffuse electron sources. W.W. performed MC simulations and analysis. D.S., P.S. and T.Z. contributed to the preparation of Au nanoparticle mask. Z.L., R.D., Y.Z., S.M. and Y.Y. contributed to electron emitter manufacturing. K.Z., T.Z., B.W. and Q.C. contributed to the characterization. X.W., W.W. wrote the manuscript. All the authors read the manuscript and provided comments.

Competing interests

The authors declare no competing interest.

Materials & Correspondence

Correspondence and material requests should be addressed to Xianlong Wei (weixl@pku.edu.cn).

Supplementary Materials

Supplementary material for this article is available.

Supplementary Files

This is a list of supplementary files associated with this preprint. Click to download.

- SupplementaryInformation.pdf